Mediterranean Marine Science

Vol 22, No 2 (2021)

VOL 22, No 2 (2021)

Recent hydrological status of the Aegean Sea derived from free drifting profilers

DIMITRIS KASSIS, GERASIMOS KORRES

doi: 10.12681/mms.24833

Research Article

Mediterranean Marine Science
Indexed in WoS (Web of Science, ISI Thomson) and SCOPUS
The journal is available on line at http://www.medit-mar-sc.net
DOI: http://dx.doi.org/10.12681/mms.24833

Recent hydrological status of the Aegean Sea derived from free drifting profilers

Dimitris KASSIS and Gerasimos KORRES

Institute of Oceanography, Hellenic Centre for Marine Research, PO Box 712 Anavyssos, Attica 190 13, Greece

Corresponding author: dkassis@hcmr.gr

Contributing Editor: Elina TRAGOU

Received: 25 September 2020; Accepted: 17 March 2021; Published online: 13 May 2021

Abstract

Being a semi-enclosed basin of the Mediterranean Sea, the Aegean Sea has a complex hydrology that plays a significant role in the hydrology of the Eastern Mediterranean Sea. Its interaction with many sub-basins, along with its contribution towards the formation of deep and intermediate water, makes it an ideal case for the study of hydrological changes in transitional areas. Since 2010, the operational monitoring of the basin has been significantly enriched by the deployment of autonomous free-drifting profilers (Argo floats) under the framework of the newly formed Greek Argo Research Infrastructure activities. In this study, the hydrological status of the area is examined for the period 2010-2017 using the temperature and salinity profiles acquired from Argo floats that operated in the basin. The profiles are analyzed together with complimentary remote sensing and model outputs datasets in order to present the spatio-temporal distribution of the co-existent water masses and shed light on hydrological features and changes that took place throughout the basin in an attempt to reassess its hydrological status during the last decade. The distribution of the physical properties in different sub-regions and their interaction is examined reconstructing a general picture of strong latitudinal gradients in the *T-S* and σ_θ fields from the upper layers towards the deeper zones. Interannually, findings indicate changes in the Aegean water masses structure within the water-column. Deep homogenization in the upper layers is recorded mainly during the winter periods of 2011-2012, 2014-2015, and 2016-2017 in the southern, central, and northern parts of the area accordingly. The observed dense water formation events, along with mixing and advection appear to alterate the water column physical properties structure and affect the dynamics of the surface and sub-surface dominant water masses in the Aegean. The results further highlight the valuable information that can be extracted from the operation of free-drifting profilers in enclosed marginal seas similar to the Aegean case.

Keywords: Hydrography; *T-S* profiles; Water formation; Water masses; Argo floats.

Introduction

The Aegean Sea is a semi-enclosed marginal basin of the Eastern Mediterranean with complex topographical and hydrological features (Theocharis *et al.*, 1993). The southern Aegean communicates with the Levantine and Ionian Seas via the Cretan Arc Straits whilst, the northern communicates with the Black Sea via the Dardanelles Straits (Fig. 1). The Aegean acts as a "host" basin for distinct water masses that interact and are either formed within, or originate from its adjacent basins. The dominant water masses that populate the water column, from the upper layers to the deep layers are: a) The high salinity Levantine Surface Water (LSW) (Lascaratos *et al.*, 1993), b) the low-salinity Black Sea Water (BSW) and Atlantic Water (AW) in the upper-layers zone (Zervakis *et al.*, 2000), c) the Cretan Intermediate Water (CIW) and the Levantine Intermediate Water (LIW) with high salinity signals (Velaoras *et al.*, 2014) and, d) the Eastern Mediterranean Deep Water (EMDW) and the Cretan Deep Water (CDW) that fill the deep layers of the basin (Theocharis *et al.*, 1993). These water masses create fronts, interact and exchange properties in the different sub-basins of the Aegean Sea determining, along with the atmospheric forcing, the physical properties distribution within the water column. Such an example is the distinct strong saline front in the northern part between the BSW and Levantine originated water masses. Being the strongest buoyant input for the wider Aegean Basin, the BSW inflow is a major factor that determines both stratification, and circulation patterns, which alternate due to the interannual variability and intense seasonality of the BSW inflow rates (Androulidakis & Kourafalou, 2011; Tzali *et al.*, 2010). With regards to the North Aegean circulation patterns, coastal and rim currents, and features such as the Samothraki Anticyclone, are largely controlled by both the Dardanelles plume and wind forcing since northerly winds promote the south-westward

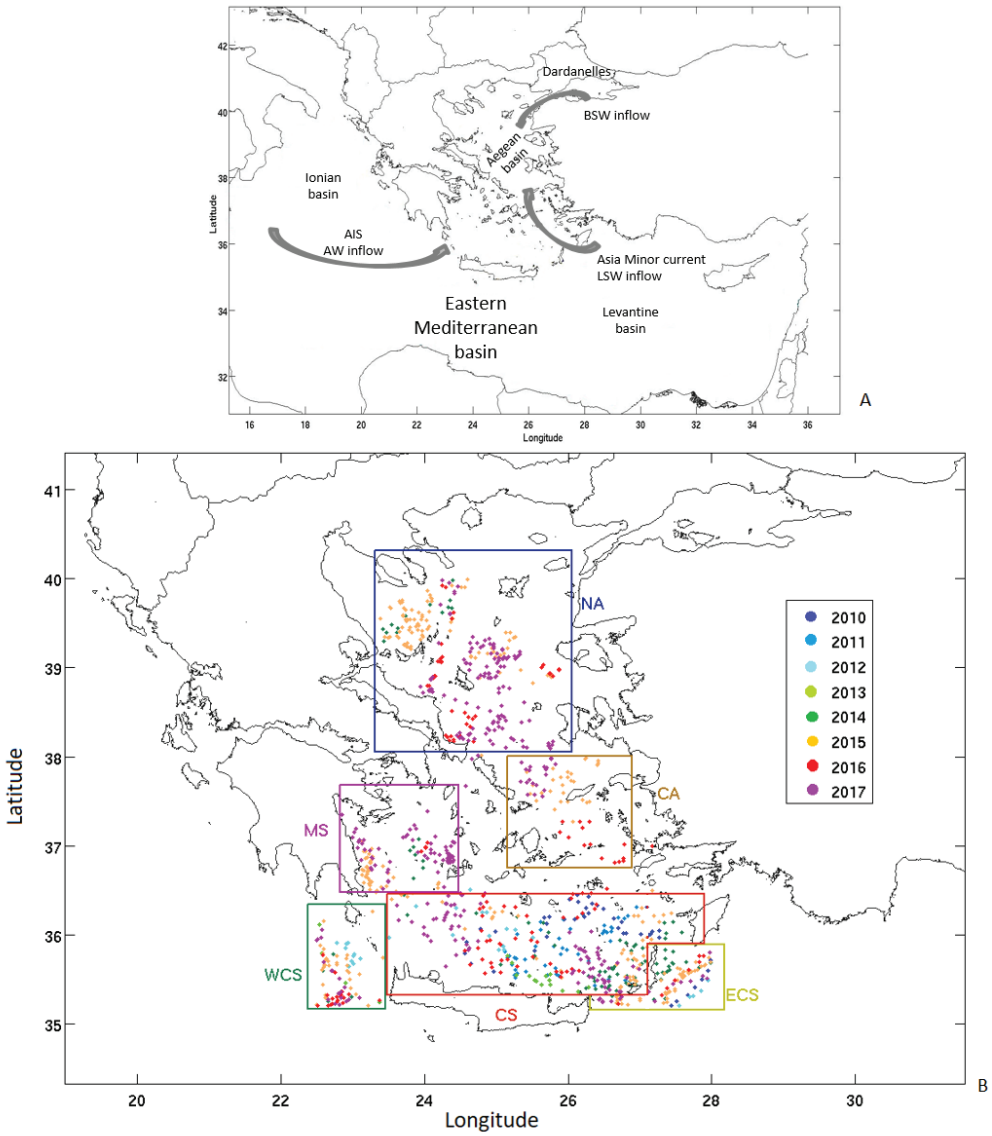

Fig. 1: A: Schematic representation of the dominant water masses input into the Aegean's upper layers; Atlantic Water (AW), Levantine Surface Water (LSW), Black Sea Water (BSW). B: Argo profiles mapped in the Aegean for the period 2010-2017. The sub-regions selected for the spatial analysis are presented: North Aegean (NA), Central Aegean (CA), Myrtoan Sea (MS), Cretan Sea (CS), Western and Eastern Cretan Straits (WCS & ECS).

transport of BSW towards the southern Aegean (Androulidakis & Kourafalou, 2011). Nevertheless, in Tzali *et al.* (2010) it is further argued that the intensity of BSW inflow may determine the general circulation of the North Aegean overpowering the wind and thermohaline forcing whilst, in Tragou *et al.* (2003) it shown that the vertical buoyancy fluxes across the upper and intermediate layers of the North Aegean determine the dense water exchange rates between the northern and southern Aegean.

Focusing on such large scale water mass exchanges and production, the most important feature of the Aegean Sea is the Dense Water Formation (DWF) events depicted in the area, identifying it as one of the major sources of deep water masses for the wider area (Theocharis *et al.*, 1999). Regarding the latter, it was in the early 1990s when a dramatic climatological and hydrological transient was observed in the Eastern Mediterranean. The transient known as the Eastern Mediterranean Transient (EMT) (Theocharis *et al.*, 1993; Roether *et al.*, 1996; Klein *et al.*, 1999; Malanotte-Rizzoli *et al.*, 1999; Lascaratos *et al.*, 1999) resulted in a massive dense water outflow from the Aegean to the Ionian and Levantine deep horizons via the Cretan Arc Straits. The event has been described as one of the most intensive DWF events that had taken place during the last decades in the Aegean basin. The Aegean undertook the role that was previously assigned to the Adriatic and became the new major source of deep water for the Eastern Mediterranean alterating the hydrology of the wider area. During the EMT, large amounts of CIW and CDW spread out from the Aegean's southern straits into the Ionian and Levantine basins occupying the deeper layers and lifting the pre-existing EMDW by several hundreds of meters (Roether *et al.*, 2007). Studies on the EMT have associated the event with several mechanisms related to meteorological anomalies, alternation of the basin's general circulation patterns, climatic variability, etc., (Theocharis *et al.*, 1999; Lascaratos *et al.*, 1999; Zervakis *et al.*, 2000; Tsimplis & Josey, 2001;

Roether *et al.*, 2007; Skliris, 2014). After the late 90s, the DWF events in the Aegean decreased, however, the area has been reported to have returned to a similar status of reoccurring DWF events during the last decade (Cardin *et al.*, 2015; Schroeder *et al.*, 2013) with DWF preconditioning being identified in the Aegean Sea (Kassis *et al.*, 2016; Kassis *et al.*, 2015; Velaoras *et al.*, 2014). Several recent reports have suggested that the Eastern Mediterranean is again presenting processes and EMT-like events, although at a lower intensity (Velaoras *et al.*, 2015; Cardin *et al.*, 2015).

The introduction of autonomous free-drifting profilers (Argo floats) in marginal seas has significantly enriched oceanographic monitoring and produced enhanced datasets during the last decade. Such evolution is the outcome of the combined activities of Euro-Argo Research Infrastructure and the National Argo initiatives. For enclosed under-sampled seas like the Aegean, the Argo monitoring coverage provided us with new records of the physical properties of the water-column. This information is extremely valuable and allows for more enhanced oceanographic studies regarding this area which is characterized by the aforementioned complexity. Taking advantage of these newly-introduced datasets, with this study we are attempting to update the current hydrological status of the Aegean Sea by assessing and analyzing the latest accumulated Argo profile data in order to describe the area's recent hydrological evolution. The spatiotemporal changes and trends of the thermohaline properties are investigated through the analysis of the acquired profiles, along with satellite and model data, during an 8-year (2010-2017) period. The dominant water masses signals are presented, with a focus on the area's main sub-regions, in an attempt to describe their hydrography and interaction. Taking advantage of the unprecedented coverage of field measurements in the area, we attempt to reconstruct its most recent hydrographic picture and highlight the importance and necessity for the expansion of the Argo network in marginal seas.

Materials and Methods

Argo T/S profiles

The main dataset used for this study consists of all available temperature, salinity, and pressure (*T*-*S*-*P*) profiles (1049 profiles) acquired from Argo floats since 2010, when the first Greek Argo float was deployed in the Cretan Sea under the Greek Argo Infrastructure activities (Kassis *et al.*, 2015), and until the end of 2017. The area of study consists of a rectangular-shape area from 22.25° E to 28° E and 35.2° N to 40.5° N. In total 1049 profile data were acquired from the Coriolis Data Assembly Centre (www.coriolis.eu.org/Observing-the-Ocean/ARGO). Only *T*-*S*-*P* values that have passed the automatic quality control procedure and were flagged as "good" (Wong *et al.,* 2020) were used for further analysis that also included a delayed-mode assessment of the data as described in Kassis *et al.* (2020). All the Argo profilers are equipped with the SBE 41/41CP CTD (Conductivity, Temperature, Pressure) pumped MicroCATs (www.seabird.com/products), with accuracies of 0.002° C for *T*, 0.005 psu for *S* and 2.4 dbar for *P*. However, the estimated accuracy for operating floats for practical salinity is approximately 0.01 psu (Riser *et al.*, 2016). The floats in the Aegean are configured to perform five-day cycles, drift at 350 m depth, and acquire profiles from 1,000 m depth to the surface, according to the MedArgo specifications (Poulain *et al.*, 2007).

Before the data analysis, a further assessment of the profile data was performed, by applying additional statistical checks and visual inspection, to exclude dubious data. This included a check on the profile location, the pressure monotony and the accordance of the maximum pressure with the profile's location bathymetry. Moreover, potential spikes were removed, taking into account thresholds referring to the climatology of the wider area (Kassis & Korres, 2020), whilst shallow profiles (< 100 dbar) or profiles with sparse data were excluded. A vertical interpolation was further performed using the piecewise cubic interpolation method in order to respect the data monotonicity and the local minima and maxima (Kassis *et al.*, 2015). Similarly to Kassis & Korres (2020), this study focuses on the actual field data interpretation thus, further spatio-temporal interpolation, statistical fitting, and grid production that would induce unknown errors dependent on subjected analysis choices, were avoided. This however preserved the profile distribution heterogeneity in space and time as shown in Table 1. The interpolation was applied from the depth level of 5 m down to 1000 m (values above 5 m depth were excluded due to the salinity uncertainty that is introduced from the floats' pump inactivation near the sea surface). After the interpolation, every data-point (*T*-*S*-*P*) that did not include all parameter values was excluded from further analysis. The final dataset consisted of 1024 valid profiles (approximately 4% of the values were removed due to the aforementioned data quality control procedure) and was spatiotemporally classified per year and sub-region. The area was divided into 6 sub-regions (Eastern and Western Cretan Straits, Cretan Sea, Myrtoan Sea, Central and North Aegean) according to topographic criteria and the distinct hydrological features that each area represents (Fig. 1). Parameters such as potential temperature, potential density - σ_θ, Mixed layer Depth (MLD), and Brunt-Väisälä Frequency (BVF), were also calculated for each profile whilst, a statistical analysis was also performed for the estimation of the minima – maxima, mean values, and Standard Deviation (STD), per area, year and depth level. The squared BVF field is a useful indicator for the buoyancy instabilities of the water column and it has been estimated using the following equation (eq. 1):

$$N^2 = \frac{-g}{\rho}\frac{d\rho}{dz} \qquad \text{eq. 1}$$

Where g is the gravitational acceleration, ρ the potential density and z the water depth. For the estimation of MLD, the de Boyer Montégut *et al.* (2004) method was used with joint threshold criteria of T and σ_θ of 0.2° C and

Table 1. Number of valid profiles per region and year.

Year	Eastern Cretan Straits	Western Cretan Straits	Cretan Sea	Myrtoan Sea	Central Aegean	North Aegean	Total
2010	7		37				44
2011			48				48
2012	5	10	13				28
2013		4	14				28
2014	21	4	47	8		14	94
2015	74	32	46	43	21	90	306
2016	8	22	43	5	14	53	145
2017	15	27	77	69	10	135	333
total	**130**	**99**	**325**	**125**	**45**	**292**	**1024**

0.03 kg m^{-3} respectively and surface reference level was set to 10 m in order to avoid the diurnal heating of the surface layers as described in Kassis *et al.* (2016).

Additional supportive datasets

For the investigation of the surface temperature variability in the study area, we analysed the satellite Sea Surface Temperature (SST) anomaly field. For that scope, the Copernicus Marine Environment Monitoring Service (CMEMS) reprocessed L4 SST dataset was used. The product provides the Mediterranean SST anomaly from the CNR-ISMAR-GOS Pathfinder pentad climatology (Pisano *et al.*, 2016; Nardelli *et al.*, 2013). This dataset is a bias-corrected version of the CMEMS NRT L4 AVHRR data at a resolution of 0.0417° × 0.0417° along with the error estimation dataset. The accuracy of the SST NRT L4 products has been assessed and the mean bias and standard deviation error for the MED HR NRT L4 product have been estimated using a comparison to independent drifter data for the period January-December 2014 which were provided by the CMEMS-OSIQUID-010-001-V1.2 INSITU TAC. Further information regarding the dataset along with its quality information can be found at: http://marine.copernicus.eu/documents/PUM/CMEMS-SST-PUM-010-004-006-012-013.pdf, and

http://marine.copernicus.eu/documents/QUID/CMEMS-OSI-QUID-010-004-006-012-013.pdf

Additional to the SST data analyses, the air temperature anomaly field has been examined over the study period. For this scope, we retrieved data from NOAA National Centers for Environmental Information, Climate at a Glance: Global Time Series, published December 2020 (https://www.ncdc.noaa.gov/cag/). The temperature anomaly data come from the Global Historical Climatology Network-Monthly (GHCN-M) data set and International Comprehensive Ocean-Atmosphere Data Set (ICOADS). The two datasets are blended into a single product to produce the combined global land and ocean temperature anomalies with respect to the 1981-2010 base period. More information on these datasets can be found at https://www.ncdc.noaa.gov/monitoring-references/faq/anomalies.php.

For the investigation of the surface and sub-surface salinity field in the North Aegean, the CMEMS product MEDSEA_MULTIYEAR_PHY_006_004_E3R1 is used (Escudier *et al.*, 2020). This physical reanalysis product is generated by a numerical system composed of a hydrodynamic model, supplied by the Nucleous for European Modelling of the Ocean (NEMO) and a variational data assimilation scheme (OceanVAR) for temperature and salinity vertical profiles and satellite Sea Level Anomaly along track data. The model horizontal grid resolution is 1/24° (ca. 4-5 km) and the unevenly spaced vertical levels are 141. Further information and details regarding this product are available at http://marine.copernicus.eu/documents/PUM/CMEMS-MED-PUM-006-004.pdf;

http://marine.copernicus.eu/documents/QUID/CMEMS-MED-QUID-006-004.pdf; https://doi.org/10.25423/CMCC/MEDSEA_MULTIYEAR_PHY_006_004_E3R1.

Results

Physical properties distribution in the water column

Regarding the whole area of study, temperature and salinity ranges were calculated for different depth zones. Remarkably, high spatiotemporal variability is depicted in the water column and wide ranges are recorded for both properties. Thus, in the surface zone (5-50 m), potential *T* and *S* span from 13.02° C to 27.93° C and 36.01 psu to 39.54 psu respectively whilst, for the sub-surface layer (50-150 m) these ranges are 12.99° C to 25.44° C and 37.17 psu to 39.69 psu. Accordingly, in the intermediate (150-350 m) and deep-intermediate (350-650 m) zones, the ranges are 13.32° C to 17.93° C, 38.4 psu to 39.37 psu, and 13.52° C to 16.17° C, 38.76 psu to 39.24 psu respectively. For the deeper zone (650-1000 m) the estimated ranges are 13.34° C to 14.89° C and 38.73 psu to 39.12 psu. The wide range of *T*-*S* is associated with seasonal and inter-annual variability and the different hydrological characteristics of the Aegean's sub-regions. Regarding the latter, large differences are presented for both properties between the southern and the northern part. These are regulated from both internal mechanisms of surface water

formation, such as precipitation and evaporation fluxes, and the surface water inflow from the adjacent sub-basin.

Water masses in the Aegean's sub-basins

Signals of the dominant water masses have been identified within the different sub-basins of the Aegean Sea. In the northern part, there is the direct effect of Dardanelles BSW outflow, marked by its characteristic low salinity signal, which also affects the central and southern Aegean waters. In the Cretan Sea, there is a similar signal associated with the AW intrusion from the west and a high salinity signal associated with the LSW from the east. In the Cretan basin, warm and high salinity water masses dominate the upper layers throughout the whole period of study whilst, in the North Aegean the cold and fresh water signals alternate seasonally and interannually. The average temperature profiles for each region indicate strong horizontal gradients between northern and southern areas that reach 1.5° C for depths below 100 m (Fig. 2A). The average salinity profiles also present differences especially in the upper and deep layers (Fig. 2B). Especially in large depths of the northern part, salinity is presented noticeably higher. Accordingly, the water density of the deep zones in the North Aegean is considerably higher as a result of the presence of colder and more saline water masses (Fig. 2C). However, these large differences are mainly assigned to the lower temperatures recorded in the northern part (Fig. 2D). The Myrtoan and Central Aegean sub-regions present intermediate characteristics between the Cretan and North Aegean. However, in the deep layers, their physical properties are similar to the ones in the Cretan Sea (Fig. 2). The Theta-S diagram constructed from all *T-S* measurements in each sub-region highlights the different status of the thermohaline properties regarding the geographical area and depth zone (Fig. 2D). In this graph, only values below 100 m are plotted in order to avoid the representation of intense seasonal variability. The results confirm the previously observed differences between Cretan and North Aegean in the 100-500 m and 500-1000 m zones. In the upper zone (100-500 m), the Cretan water masses depict increased salinity and potential temperature, reflecting strong signals of LIW/CIW. For the North Aegean, this zone is more extended in terms of the *Theta-S* field depicting water masses similar to Myrtoan and Central areas including LIW masses and signals of BSW which has deepened its core below 100 m. In the deeper zone, the σ_θ potential density of the Cretan Sea water masses slightly exceeds 29.2 Kg m^{-3} on the contrary, the recordings in the northern sub-basin present masses significantly denser that reach 29.45 Kg m^{-3}.

Variability of the salinity field

The inter-annual variability of the salinity field in each sub-region has been investigated for different depth

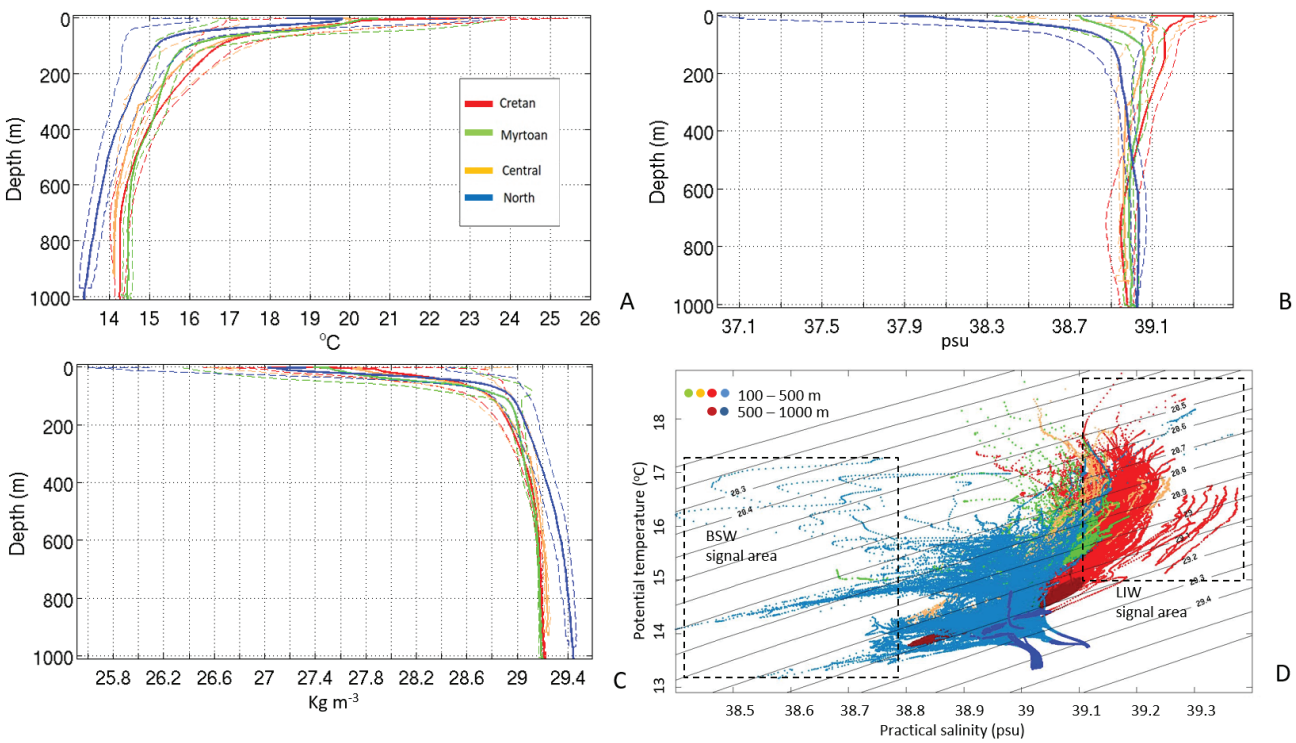

Fig. 2: Average profiles with their associated STD for potential temperature (A), salinity (B), potential density (σ_θ) (C), and Theta-S diagram (D) for the Cretan Sea (red), Myrtoan Sea (green), Central Aegean (orange), and North Aegean (blue) for the period 2010-2017. In D the light colours represent the 100-500 m layer whilst dark colours represent the 500-1000 m layer (only for the Cretan and North Aegean cases). The black-dotted rectangular areas are indicative of the Black Sea Water (BSW) and Levantine Intermediate Water (LSW) Theta-S signals.

layers of the water column (Fig. 3). For simplicity reasons, only the average salinity is presented in this graph excluding the STD which is in general low (<0.09 psu) for all sub-regions and depth zones, with the exception of the North Aegean surface zone in 2015 and 2016 when the STD recorded 0.1397 psu and 0.1328 psu accordingly, and was most probably related to the spatially heterogeneous profile distribution across the area. According to this analysis, the salt content of the sea surface does not present large interannual variability in the southern areas including the Eastern and Western Cretan Straits where the LSW dominates. Especially regarding the Eastern Cretan Straits and the Cretan Sea, the surface salinity field is ranging between 39 psu and 39.25 psu with the higher values depicted in the former reflecting the strong influence of the LSW inflow in the south Aegean from its eastern borders (Fig. 3A). In the Cretan basin, the high salinities (approximately 39.4 psu) recorded in 2010 are significantly reduced in the following years remaining lower than 39.27 psu (Fig. 3A). For the central and northern areas, the available data after 2014 suggest a general increase of the salinity that is probably related to significantly weaker BSW presence at its western part where 2014 and 2015 profiles overlay (Figs. 1B, 3A). However, the abrupt salinity increase that is recorded in the North Aegean during 2017 is also related to the increased number of profiles at the south-eastern borders of the sub-region. The surface layers of these areas are less affected by the BSW presence, on the contrary, LSW presence is stronger compare to the more high latitudes. In previous studies, it has been demonstrated that the BSW-LSW front oscillates between southeast of Lemnos island in the summer period, to the northeast of the island in winter, a fact that is attributed to the Etesian winds (northerlies) that dominate during the late summer period (Zervakis & Georgopoulos, 2002). An investigation on the sub-surface salinity field, as derived from model estimations, shows good agreement with these findings. The monthly average salinity field in August, when the BSW presence is particularly strong (Tzali *et al.*, 2010), presents a distinct latitudinal gradient at the eastern part with salinities ranging from 39.2 in the south to 34.8 psu in the north whilst, in the western part values range between 37-38 psu accordingly (Fig. 4). Moreover, an increase in salinity is shown after 2014, which is the year with the strongest recorded BSW signal (Fig. 4). More specifically, at the entrance of the Dardanelle Straits (40° N, 26° E) salinity at the 10 m depth level increases from 36.4 psu in August 2014, to more than 37 psu in August 2016 (Fig. 4I).

In the underlying zone, between 200 m and 300 m depth, the major changes in the average salinity are depicted in the Cretan Sea (Fig. 3B). The recorded decrease of approximately 0.13 psu between 2010 and 2013 depicts the weakening of the LIW core that was previously dominant in the area whilst, for the Cretan Straits an increase has been recorded during the same period. In the following years, a general increase is presented however, the salt content remains well below the 2010 status. In the Myrtoan Sea, Central, and North Aegean the available data suggest relatively high variability with salinity peaks during 2015 and 2016 accordingly (Fig. 3B).

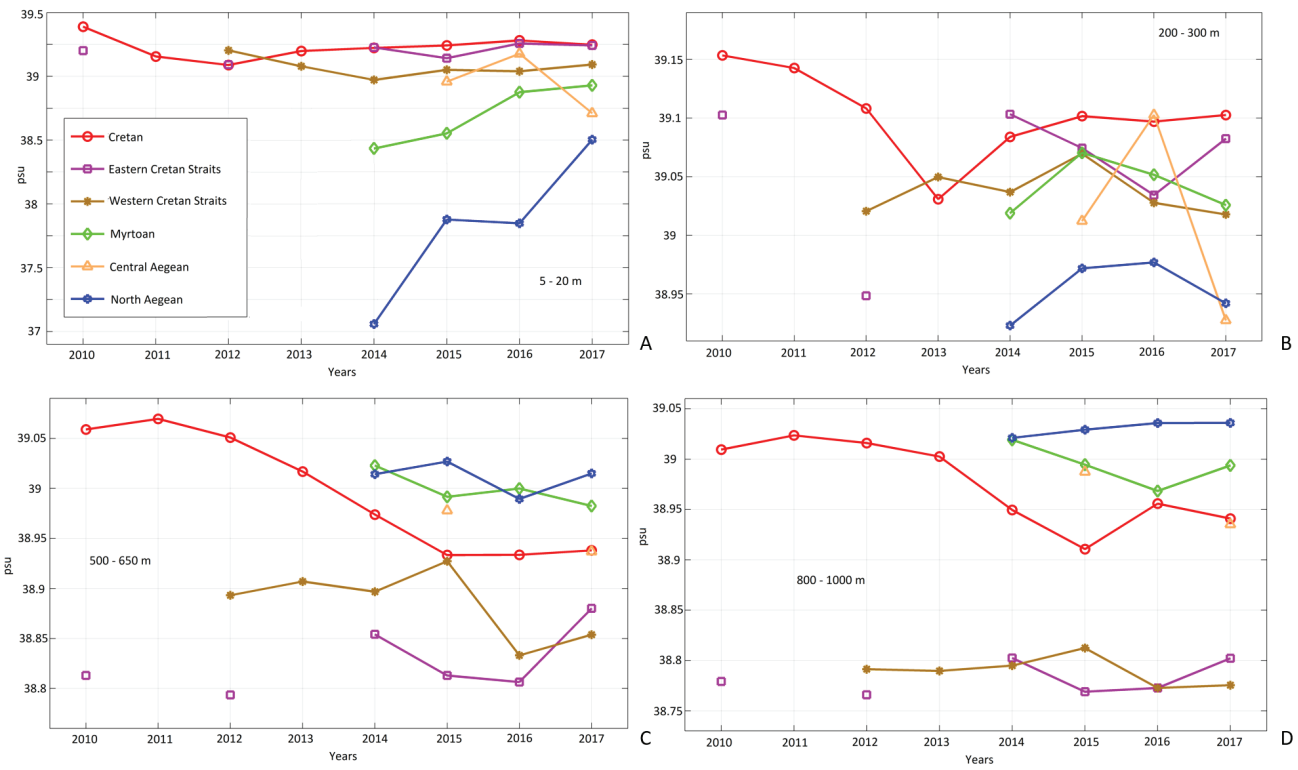

Fig. 3: Yearly salinity average per depth layer and sub-region during the period 2010 -2017. A: 5-20 m, B: 200-300 m, C: 500-650 m, D: 800-1000 m. The associated STD has been estimated to be less than 0.09 psu in all cases with the only exception of North Aegean surface zone (A) when in 2015 and 2016, it exceeds 0.13 psu.

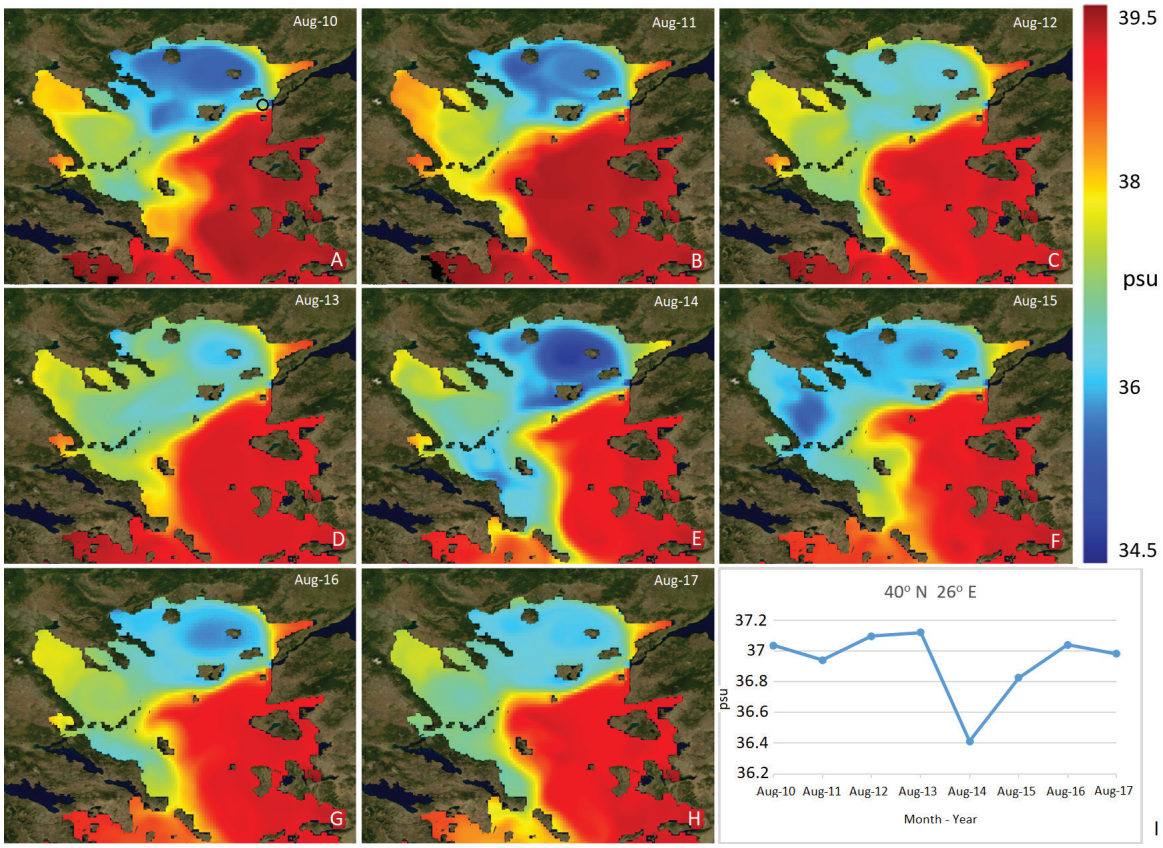

Fig. 4: Monthly average sub-surface (10.54 m depth) salinity field of the North Aegean produced by numerical simulation for the following time periods: A) August 2010, B) August 2011, C) August 2012, D) August 2013, E) August 2014, F) August 2015, G) August 2016, H) August 2017. In panel I, timeseries of the same field are presented for the location 40° N, 26°E, indicated by the black circle in panel A. The salinity field is acquired from the CMEMS product: MEDSEA_MULTIYEAR_PHY_006_004_E3R1

A more persistent salinity decrease, with an approximate rate of 0.025 psu yr^{-1}, is presented in the 500-650 m depth zone in the Cretan basin from 2011 until 2015, indicating a major change in the water masses occupying these layers (Fig. 3C). Such a decrease is also evident in the deeper zone (800-1000 m) (Fig. 3 D), resulting in an overall decrease of the salt content especially in the southern areas of the Aegean. In order to visualize the spatial salinity distribution in the area of study, all the salinity records are classified into low –medium– high values and plotted for distinct depth levels (Fig. 5). This distribution clearly shows the south to north negative salinity gradient in the upper layers (Fig. 5A). This picture is reversed for the deep layers where a positive latitudinal salinity gradient is present and described by lower salinities in the southern and higher salinities in the northern part (Fig. 5D). More specifically, the 20 and 50 m levels depict high salinity records reflecting the dominance of LSW not only in the southern part but also in the Central Aegean and the centre of the North Aegean basin. In the latter, low salinity signals are also recorded, representing strong BSW presence which follows a general cyclonic pathway along the western Aegean coast towards the Myrtoan Sea (Fig. 5A). This is in good accordance with previous studies describing the pathways of the BSW in the western half of the Aegean basin (Kourafalou & Barbopoulos, 2003). Regarding the 200 and 300 m levels (Fig. 5B), the high salinity signal of LIW is apparent mainly in the southern part with some additional records in the eastern part of the Central Aegean area. In the north, the low salinity signals well below 38.9 psu, which are recorded in the 200 m and 300 m levels, probably depict deep homogenization that has deepened the BSW core (Fig. 5B). Regarding the 500 and 600 m levels, a wide span of salinity values is apparent in the Cretan Sea and its southern borders, reflecting intense inter-annual variability and water masses exchanges from the Cretan Straits (Fig. 5C). In the North Aegean basin, high salinity is recorded in its central and north-western parts. The same picture is presented in the deeper levels (800 m and 1000 m) however the recordings are fewer (Fig. 5D) due to the shallow bathymetry in large parts of the Aegean basin.

The intense variability of the salt content in the intermediate and deep layers of the Cretan Sea, as depicted in Figures 3 and 5, is further examined with the statistical analysis of the salinity profile data in the area. The yearly salinity average depicts a strong salinity shift in the whole water-column which is particularly interesting for the 500-900 m depth zone where it depicts an average decrease of more than 0.15 ± 0.02 psu between 2011 and 2015 (Fig. 6A). In this zone the intense salinity shift is observed in 2013, however, for the overlying layers, it started during 2012. During this year and especially in 2013, the LIW core disappears from the area's water-column thermohaline status whilst, strong signals of the slightly colder and significantly fresher Transitional Mediterranean Water (TMW) are recorded to occupy the intermedi-

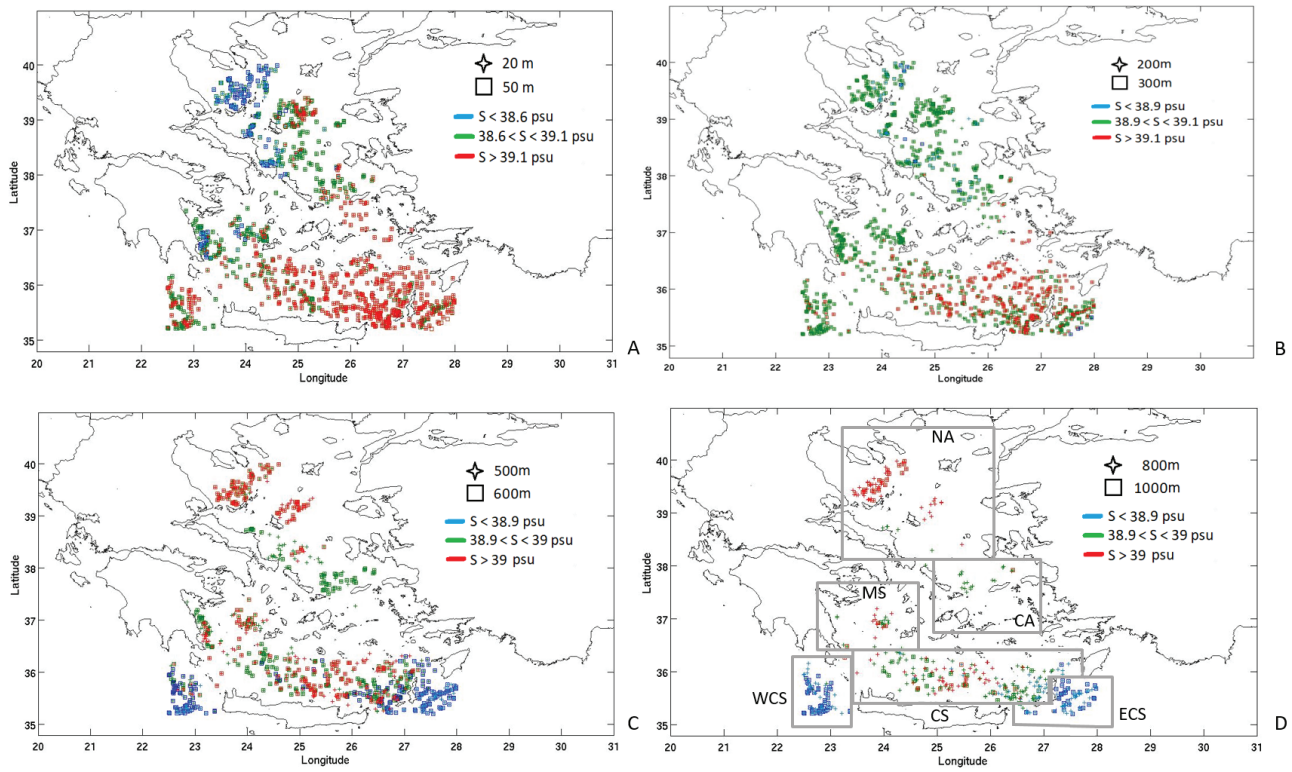

Fig. 5: Spatial salinity distribution classified in low (blue), medium (green), high (red), in different depth levels derived from all Argo float recordings for the period 2010-2017. A: 20 and 50 m, B: 200 and 300 m, C: 500 and 600 m, D: 800 and 1000 m. In panel D the examined sub-regions are indicated as in Figure 1.

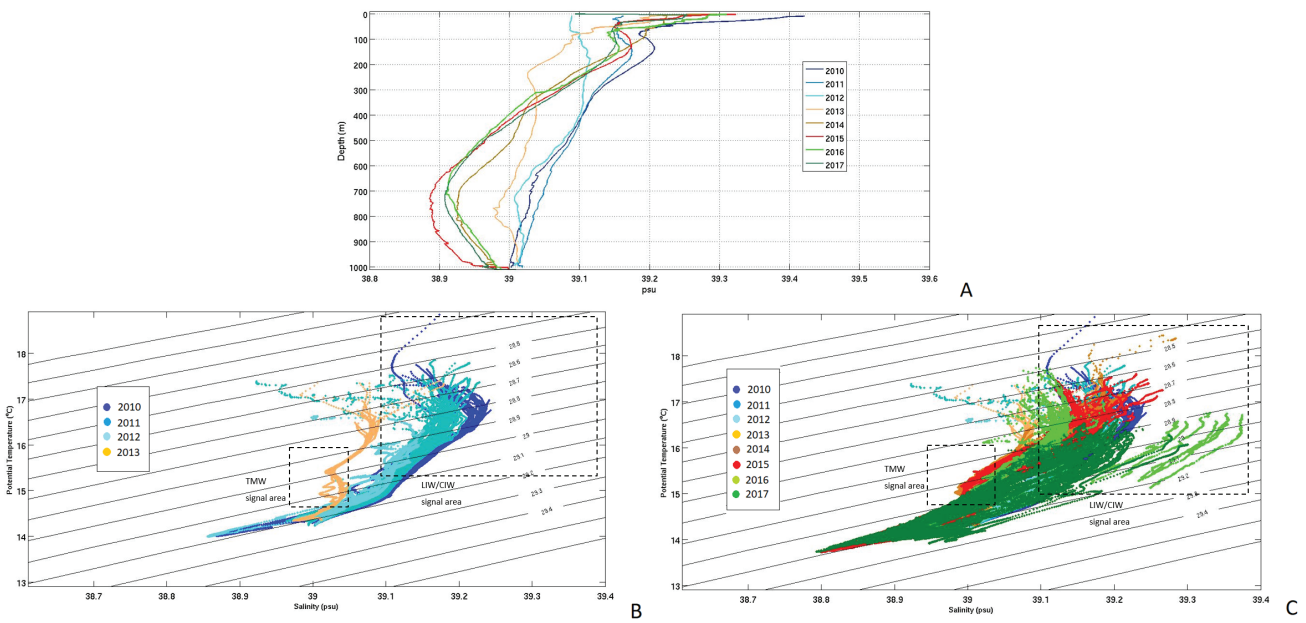

Fig. 6: Yearly average salinity profiles in the Cretan Sea (A), Theta-S diagrams in the Cretan Sea in the depth zone 100-1000 m during 2010-2013 (B), and for all years (C). The black-dotted rectangular areas are indicative of the Transitional Mediterranean Water (TMW) and Levantine or Cretan Intermediate Water (LIW/CIW) Theta-S signals.

ate and deep intermediate layers (Fig. 6A, B). During the following years the yearly average salinity profiles are similar and present a relatively weak and shallow LIW core (~ 39.14 psu at 150 m) and a strong negative halocline until the 750 m depth horizon reaching a salinity minimum of approximately 38.9 psu (Fig. 6A). However, the average profiles do not homogenously represent the salinity field for the sub-basin mainly due to the temporal heterogeneous profile distribution. The Theta-S diagram of all the profiles reveals a wide span of the *T-S* records after 2014 (Fig. 6C). During 2016, some extreme salinity signals are also observed but are only related to 5 shallow profiles at the eastern borders of the sub-basin. In 2017, the densest water masses are observed at the south-east-

ern borders of the Cretan basin with σ_θ exceeding 29.26 kg m^{-3} (Fig. 6C). In general, and especially for the years 2016 and 2017, the measurements comprise characteristics of both (pre-2012 and after-2012) periods nevertheless, it is still the latter status that dominates in the area as derived from the majority of the profiles.

Thermohaline variability at the Aegean's southern borders

In order to investigate the thermohaline status of the Aegean's southern part, the profile data from the western and eastern areas outside the Cretan basin (Fig. 1 WCS & ECS) are further processed. The associated Theta-S diagram (Fig. 7A) depicts the inter-annual variability of the two areas for the layers below 200 m. As shown, the eastern part presents a wider *T-S* distribution depicting relative warm (16.9° C maximum *T*) and high salinity (39.25 psu maximum *S*) intermediate water masses whilst, at the western part *T* and *S* do not exceed 16.52° C and 39.15 psu respectively (Fig. 7A). In these layers, the western part also depicts signals of relatively low salinity (~ 39 psu) during 2012-2013 similar to the signals observed in the Cretan basin during the same period. In the deep layers the western part presents more homogeneity with water masses reaching 29.21 kg m^{-3} maximum density during 2015, whilst in 2016 and 2017 a slight shift is observed with densities of below 29.19 kg m^{-3}. On the contrary, the eastern part is roughly divided into 3 distinct time periods (2010, 2012-2015, and 2016-2017). A major shift is observed after 2015 and up until 2017 when the low salinity and density signals are replaced by dense and saline water masses resulting in the reverse of the west-east deep horizontal salinity and density gradient. The 2014-2015 deep intermediate water masses of the eastern part are similar with the signals observed in the Cretan basin during the same period. The yearly salinity average profiles also depict these changes (Fig. 7B, C). However, it is of interest to notice the strong salinity decrease in the western part's surface layers between 2012 and 2014, the absence of a strong LIW signal in the eastern part after 2010, and the salinity increase in the deep intermediate layers of the same area during 2017 (Fig. 7B, C).

Deep convection and mixing events

The strong spatio-temporal *T-S*-σ_θ gradients depicted within the layers below 100 m reflect the basin's thermohaline circulation, and mixing processes in the water column. In order to identify the locations of DWF processes, a further analysis on the dataset has been applied that included the estimation of the MLD and the BVF frequency for each individual profile. Regarding the latter, the majority of the buoyancy instabilities in the upper layers are recorded during winter of each year due to the seasonal surface cooling. According to the represented BVF field three main periods of extended vertical instabilities are recorded (2011-2012, 2015-2016 and 2016-2017) (Fig. 8A). The relevant profile locations where negative BFVs are recorded within the upper 200 m are plotted

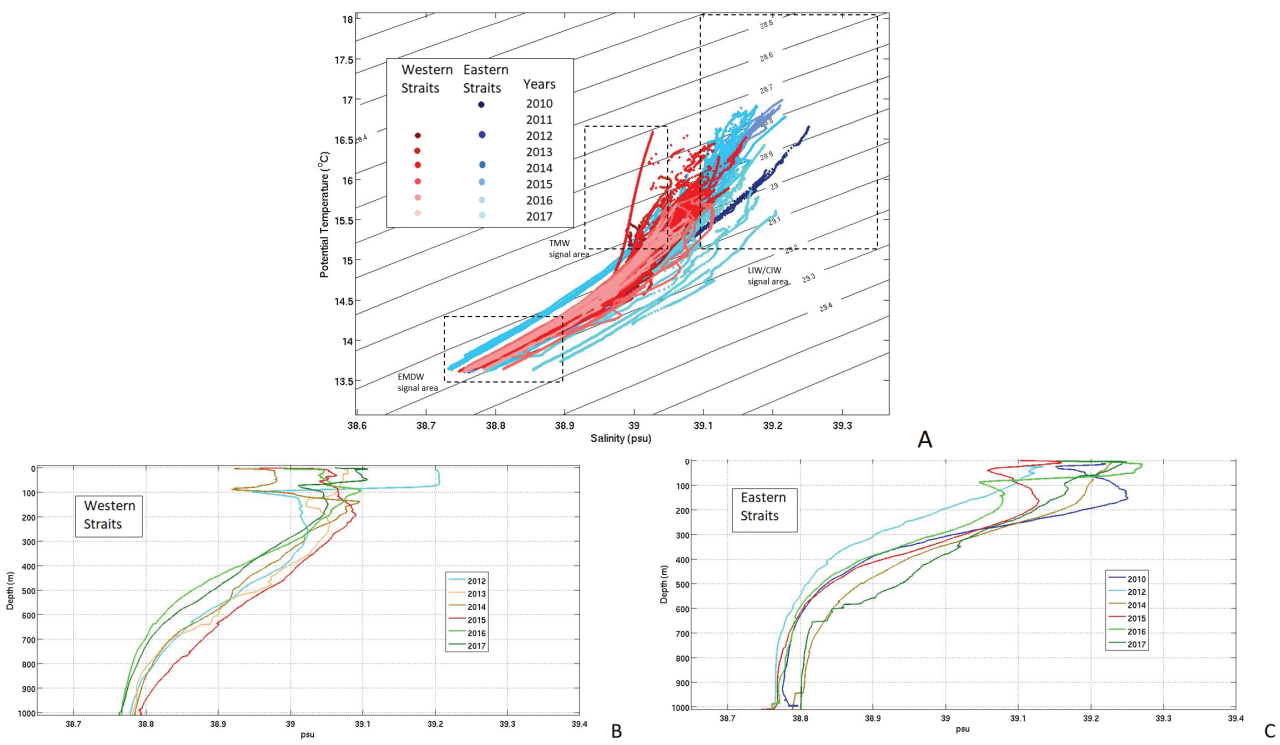

Fig. 7: Theta-S distribution per year in the Eastern and Western Cretan Straits for depths 200-1000 m (A). The black-dotted rectangular areas are indicative of the Eastern Mediterranean Deep Water (EMDW), Transitional Mediterranean Water (TMW), and Levantine or Cretan Intermediate Water (LIW/CIW) Theta-S signals.Yearly salinity average profiles in the Western (B), and Eastern (C) Cretan Straits.

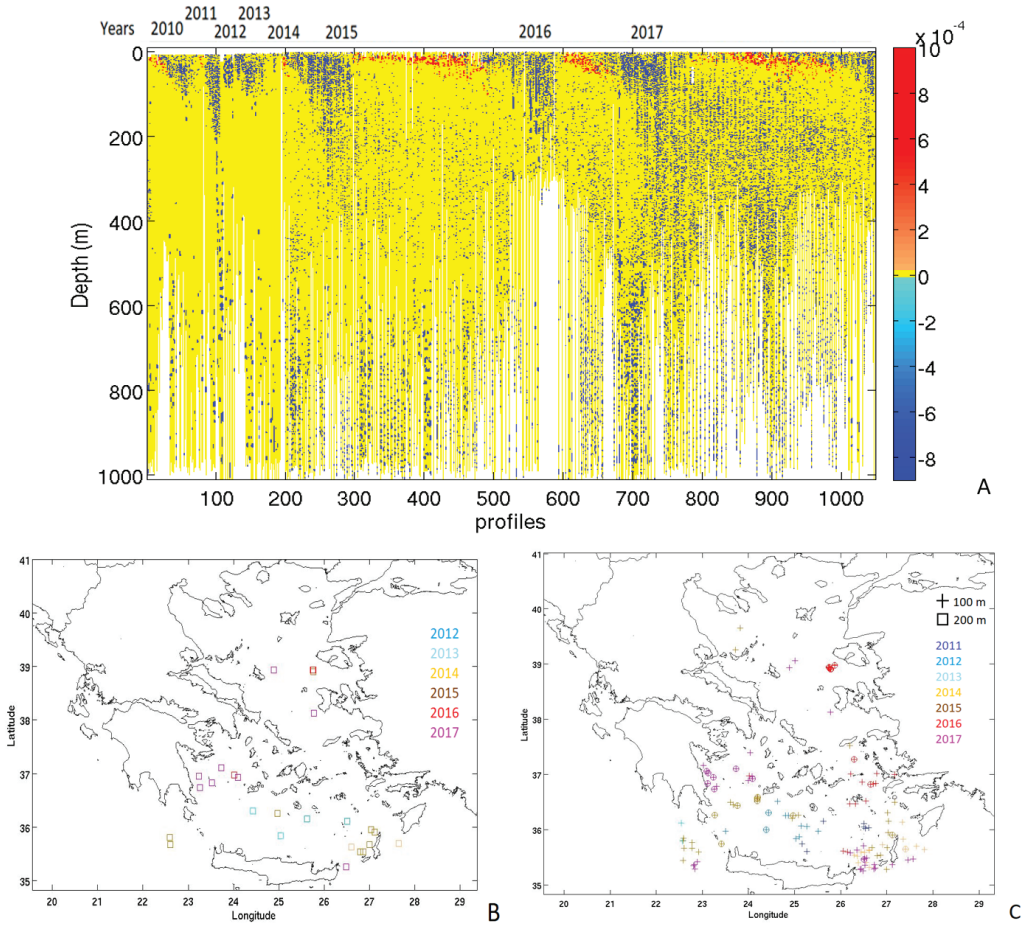

Fig. 8: Hovmöller diagram of the Brunt-Väisälä Frequency (BVF) squared for each profile (A). Profile locations for each year where BVF squared is negative within the upper 200 m (B). Profile locations for each year where the Mixed Layer Depth (MLD) exceeds 100 m (crosses) and 200 m (squares) (C).

for each year (Fig. 8B). Furthermore, the profile locations depicting MLDs deeper than 100 and 200 m were also identified and classified on a yearly basis (Fig. 8C). The co-location of the two distributions gives an idea of the convection areas due to deep homogenization. According to this, the northern Cretan Sea during 2012 and 2015, the Eastern Cretan Straits during 2015 and 2017, the southern Myrtoan Sea during 2015, 2016 and 2017, and the North Aegean during 2015 and 2017, are the main areas depicted. The majority of the events are measured after 2015 however, caution should be applied to these results, as during the period up until 2014 the available profiles were sparse, and the central and northern sub-regions have minor or no representation at all.

Sea surface and air temperature anomalies

The monthly SST anomaly, as derived from satellite data, along with the corresponding air temperature anomaly field are investigated in order to mark inter-annual signals and climatic variability over the Aegean. In Figure 9, the 3-monthly mean SST field has been reconstructed focusing on the "cold" period (January-March) of each year so as to assess possible pre-conditioning statuses for DWF. In general, positive anomalies dominate with the exception of 2012 and 2017 when extended negative values are present in the basin (Fig. 9 A-H). The estimation of the air temperature annual anomalies in the Cretan, Myrtoan, and North Aegean sub-regions depict similar signals (Fig. 9I). It is of interest to notice that the North Aegean is the area subjected to the largest variability depicting the higher and lower peaks during 2014, 2016, and 2012, 2017 accordingly (Fig. 9I). In general, the relatively low temperature records of the air-sea zone during 2012 and 2017 are a factor that probably determined the convection events described previously (Fig. 8A). Furthermore, negative SST signals depicted in the Eastern Cretan Straits in 2015, and additionally in the Myrtoan and North Aegean in 2017, are in agreement with the convection locations identified through the MLD and BVF combined analysis (Fig. 8B, C, Fig. 9F, H).

Discussion

The Argo dataset has proved a valuable source of information regarding the area's thermohaline properties distribution due to the unprecedented density of profile records. However, uncertainties may be introduced due to the inhomogeneous spatio-temporal distribution of the profiles, especially during the 2010-2014 period when the profiles

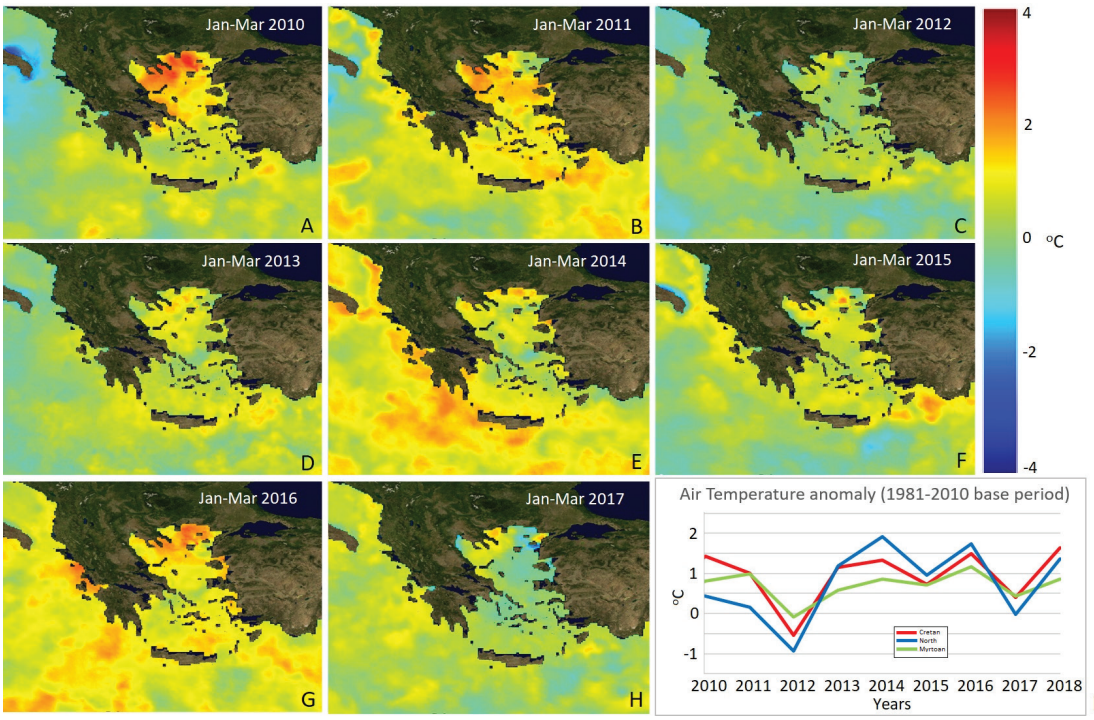

Fig. 9: Satellite SST anomaly field based on pendant climatology averaged for the January-March period of the years: A) 2010, B) 2011, C) 2012, D) 2013, E) 2014, F) 2015, G) 2016, H) 2017. In panel I, the air-temperature yearly anomaly (with respect to the period 1981-2010) is presented for the 2010-2017 period for the Cretan (red), Myrtoan (green), and North Aegean (blue) sub-regions. The SST field is acquired from the CMEMS product: CMEMS-SST-PUM-010-004-006-012-013.

were sparse. The sparsity of data has prevented the authors from interpolating the discrete data on a regular grid in order to reduce the impact of the heterogeneous spatial and temporal distribution. Thus, having acknowledged the misinterpretations induced due to the spatio-temporal heterogeneity, this study focuses on the actual recorded field values and their presentation and investigation, avoiding statistical classifications and data interpolation and extrapolation methods that can produce unknown errors dependent on subjected analysis choices and arbitrarily selected parameters. Although it is difficult to quantify the aforementioned uncertainties, the analysis of complementary numerical and satellite datasets and the level of agreement with the available *in-situ* profile data, give us a qualified picture of the adequacy of the latter.

From the data analysis presented here, important information is extracted and synthesized regarding the Aegean's recent hydrographic status. In the surface layers, high salinity signals dominate in the southern part and extend in the eastern and northern areas. These signals are associated with LSW that appear more extended especially during the early years of the study period. The LSW signals are dominated by the Asia Minor current that brings warm and saline water in the south-eastern Aegean (Fig. 1). This explains the agreement in the variability of the surface salinity field between the Cretan basin and Eastern Cretan Straits (Figs 6, 7). According to this, increased salinities are recorded in both areas in 2010, 2016 and 2017 whilst, lower values are depicted in 2012. The generally strong presence of LSW since 2010 is related with its increased inflow from the Aegean's south-east borders before and during 2010 due to, according to Kress *et al.* (2014), the general salinity increase from 2005 up until 2010 in the Levantine's upper and intermediate layers. In more recent studies, this extended presence of LSW in the Levantine and its spread, especially after 2010, towards the west, results in considerably higher surface salinity in the Aegean after 2012 (Kassis & Korres, 2020). Furthermore, the AW and BSW have depicted only a weak presence in the Cretan basin. Especially regarding AW, its absence from the Cretan Sea western boundaries is in agreement with previous studies reporting a general gradual reduction of the AW inflow in the Ionian that reaches a minimum in 2012 (Kassis *et al.*, 2017; Kassis & Korres, 2020). In the following years, only a few profiles present a weak AW signal in the Western Cretan Straits mainly during 2014. Regarding the BSW, its strong presence is observed only in the Cretan's northern and west-central boundaries towards the Myrtoan Sea especially during 2014 and 2015. This is mainly related to both BSW outflow rates from the Dardanelles mouth and the wind field. In the cases of low BSW outflow rates, the low salinity signal of the upper layers disappears whilst, the combination of strong outflow rates and northerly winds may bring brackish waters southwest, towards the Evia Island area (Androulidakis *et al.*, 2012a; Zervakis & Georgopoulos, 2002). In the underlying layers, a strong LIW core is observed during 2010-2011 in the South Aegean part related to increased LIW production in the Levantine during the previous period, and associated with the contemporary anticyclonic phase of the North Ionian Gyre (NIG) during 2011 (Ozer *et al.*, 2017). Nevertheless, the LIW core is presented shallower (~ 170 m) and extended only towards the central-east-

ern parts of the Aegean where is recorded weakened until 2016. In the same depth horizon, low salinity signals in the North Aegean are related to the deepening of the BSW after intense surface cooling and vertical mixing mechanisms that followed mainly due to wind force. The upper layers deep homogenization is mainly depicted in the southern borders of the North Aegean after 2015 when the surface BSW signal weakens. On the contrary, its strong presence, especially during 2014, acts restrictively over convection processes since, as described in relevant studies, it can regulate DWF events acting as an insulating surface lid (Zervakis *et al.*, 2000).

In general, the salinity spatial distribution presents a primary south – north, and a secondary east – west positive gradient for the first few hundred meters of the water column. Below the 500 m depth horizon this picture is reversed and the gradients become negative. In the 500-650 m layer certain areas depict large salinity variability as a result of DFW events or horizontal advection that follows DWF events. Such an example is the Myrtoan basin where the relatively warm and saline deep water is a result of deep convection that took place in its southern borders especially during 2015 (Kassis *et al.*, 2016). It is important to notice that the Myrtoan sub-region also communicates with the Cretan basin through its deeper layers. This explains the similar characteristics of the two sub-basins deep water masses since, after convection events, interaction and mixing are possible through horizontal advection. On the contrary, for the North Aegean, the deep layers are secluded from the southern parts, exchanging properties only through vertical mixing with the intermediate layers whilst, dense water exchanges between the northern and southern Aegean take place in the same layers due to buoyancy fluxes (Tragou *et al.*, 2003; Zervakis *et al.*, 2003). Thus, the main interaction with the southern sub-regions is through the upper and intermediate layers circulation. Due to the general cyclonic circulation pattern, the northern part receives from the Central Aegean warmer and saline water masses (LSW & LIW) and feeds the Myrtoan with cold and fresher waters through the sub-surface circulation. The North Aegean, deep convection events that took place during the previous period resulted in the dense water masses filling its deep sub-basins. For the period of study, the colder and saltier water masses below 450 m depth between 2015, 2016, and 2017, along with the extended MLDs and the negative BVFs, suggest DWF events do not seem to penetrate the 650 m depth horizon. In Velaoras *et al.* (2017) such events are explained in the North Aegean as being due to the exceptionally cold winter of 2016-2017 that resulted in heat loss comparable to the EMT period (1992-1993). This is in agreement with our investigation on the SST and air temperature anomaly fields that identifies the winters of 2011-2012 and 2016-2017 as heat loss periods that resulted in increased DWF events. Previously to our study period, atmospheric conditions have been reported to play a major role on DWF such as the year 2003 when low winter temperatures resulted in strong buoyancy losses and new dense water masses were produced in the surface and intermediate layers of the northern Aegean area (Androulidakis *et al.*, 2012b). According to our data analysis, the locations of the DWF events are traced to the central-east and central-west parts of the North Aegean for the winters of 2015-2016 and 2016-2017 accordingly (Fig. 8B, C). Apart from the seasonal surface cooling, these events have been accentuated by the aforementioned weakening of the BSW presence and possible wind-induced mixing that resulted in higher surface salinities which favoured the pre-conditioning of the area for DWF. Reduced BSW inflow rates that result in weak stratification of the upper layers, coincide with maximum atmospheric cooling and thus facilitate vertical mixing (Tzali *et al.*, 2010). This is accentuated by increased LSW presence. In Androulidakis *et al.* (2012b) it is argued that in 2006, the intrusion of more saline Levantine waters increased the sigma–theta of the south North Aegean region, creating precondition factors for DWF events. On the contrary, as suggested in the same study, the wide spreading of BSW may affect the MLD variability in the area, promoting the stratification of its upper layers and counteracting convection processes. In agreement with the latter, our analysis further shows that in areas where a wide salinity and density variation is recorded, extended MLDs are present (Fig. 5, 8). However not all areas host actual DWF locations since there are examples where the previously formed water is advected from a neighbouring area (Marshall & Schott, 1999; Schroeder *et al.*, 2017). These are the cases of the Cretan basin and the Eastern Cretan Straits especially after 2015. Both signals of the aforementioned strong LIW, and the CIW that was previously produced from DWF events in the Cretan basin (Schroeder *et al.*, 2013; Kassis *et al.*, 2015), become abruptly weaker after 2011. This abrupt salinity decrease reflects an intensified outflow of these water masses towards the Cretan Straits (Kassis *et al.*, 2016). At the same time, the significantly fresher and slightly colder TMW entered the Cretan basin compensating the outflow (Fig. 6). The presence of TMW alternated the hydrography of the sub-basin and can act as a tracer for DWF events in the Aegean Sea (Velaoras *et al.*, 2015). In this study, the profile analysis in the south Aegean is expanding the picture of the extended low-salinity signals in the Cretan basin. These signals are related to advection processes and water masses exchanges between the Cretan basin and its adjacent sub-basins (Myrtoan Sea, South Ionian, and Eastern Levantine). The beginning of the *T-S* shift is traced early in 2012 in the upper layers (100-300 m) especially for the salinity field and is most possibly related to subsurface eastward inflow from the Western Cretan Arc that presented intermediate water masses with similar thermohaline properties. During the following year, the salinity decrease is observed deeper (400-900 m), and the recorded *T-S* properties are similar to the Eastern Straits, suggesting a westward inflow in the Cretan basin (Fig. 7). In recent years (2015-2017) the area presents a wide range of salinities comprising both statuses (before and after 2012). Deep horizontal mixing is not favoured at the southern borders of the Cretan Basin due to the shallow topography at the Cretan Straits. This is the reason why the deep layers inside and outside

the Straits present different thermohaline characteristics. On the contrary, for the upper and intermediate layers, the picture is more homogenized due to water exchange and mixing. The profile data analysis for the Eastern and Western Cretan Straits also suggests inter-annual variability. In general, the western part indicates a more homogenized *T*-*S* distribution, with a gradual decrease of the density and salinity of its deep layers after 2015 that is possibly related to the recessed inflow of LIW/CIW from the Cretan basin and the strong presence of EMDW and deep water that was produced in the Adriatic (Fig. 7). On the contrary, for the intermediate and deep layers of the eastern part, two peaks in the density-salinity fields are depicted. The first in 2014, related to exchanges with the Cretan Sea through the Eastern Cretan Arc, and the second in 2017 related to the deep homogenization of the water column that is traced in the area. In general, the two sub-regions present an inter-annual west-east salinity gradient that is positive in the upper layers and negative in the deeper zone.

Conclusions

The recent Aegean hydrological structure derived from the profile data analysis depicts spatiotemporal variability of the basin's physical properties throughout the examined period. Especially with regards to the salinity distribution, this is determined by interannual changes that took place in the wider area. In general, the results highlight a strong positive latitudinal salinity gradient in the upper layers that is reversed towards the deeper zones. This fact, along with the presence of colder waters that are recorded in the northern areas is translated into an increase, with depth, of the density gradient between north and south. A secondary west-east positive salinity gradient that also becomes negative in the deeper layers is further observed. In general, the strong horizontal thermohaline gradients at the deep layers are a combined reflection of convection events that accumulated deep water masses with different characteristics and advection processes between the different sub-regions. The most important features revealed in the different sub-regions are the following:

- The northern part presents higher variability both in *T* and *S* with strong seasonal signals of BSW mainly during 2014 that also reached the Myrtoan Basin. The BSW signal is weakened after 2014 most possibly reflecting reduced inflow from the Dardanelle Straits. Intense seasonal homogenization of the North Aegean upper layers is observed that deepens the BSW core below the 200 m depth horizon.
- The increase in salinity of the intermediate layers in the Myrtoan Sea during 2015 and in the Central Aegean in 2016 is related to the deep mixing that occurred at the beginning of these years in each area.
- In the Cretan Sea, the σ_θ potential density of deep water masses is far below the densities observed during the EMT period. Moreover, the DWF events that took place in the area after 2011 were weak and did not ventilate the deep parts of the basin. Both facts suggest a relaxation of the Cretan Sea in terms of deep convection events.
- Although the Cretan Sea, sub-surface water mass structure does not resemble an EMT-like status, the increased salinity of the surface layers due to the dominance of LSW and the absence of strong BSW and AW signals ensure the area is pre-conditioned for DWF events.
- The dramatic change of the water mass structure of the Cretan basin had already started in early 2012 associated with upper layers eastward inflow whilst, the deep transition is mainly related with the eastern part.
- Outside the Cretan Basin, the variability of both *T* and *S* is strongest in the eastern part which presents significantly less dense intermediate and deep water in 2014 than in 2017. The 2014 deep-intermediate water masses have filled large parts of the Cretan Basin. On the contrary, in the western parts, the water mass exchanges are mainly depicted in the upper-intermediate layers.
- The main DWF events recorded in the area are in the Cretan Sea during 2012, in the Myrtoan Sea and outside the Cretan Straits during 2015 and in the North Aegean and the Myrtoan basins during 2016-2017.
- The latest profile data from Argo floats has proved a valuable source of information regarding the hydrography of the Aegean Sea. Although until 2014 the profiles are sparse, the increased data coverage during the following years can lead to conclusive results regarding the spatio-temporal variability and trends of the basin's physical properties. This fact underlines the necessity of increased float coverage in the marginal seas that will lead to enhanced monitoring and investigation of variable and transitional areas like the Aegean.

Acknowledgements

The Argo profile data are acquired from the Argo GDAC and are available at: http://www.argodatamgt.org/Access-to-data/Access-via-FTP-on-GDAC. These data were collected and made freely available by the International Argo Program and the national programs that contribute to it (https://argo.ucsd.edu/data/acknowledging-argo). The Argo Program is part of the Global Ocean Observing System. ARGO DOI http://doi.org/10.17882/42182.

This study has been conducted using E.U. Copernicus Marine Service Information and the following products are used: http://marine.copernicus.eu/documents/PUM/CMEMS-SST-PUM-010-004-006-012-013.pdf; http://marine.copernicus.eu/documents/PUM/CMEMS-MED-PUM-006-004.pdf.

For atmospheric dataset the following datasets from NOAA National Centers for Environmental information are used: Global Historical Climatology Network-Monthly (GHCN-M) data set and International Comprehensive Ocean-Atmosphere Data Set (ICOADS). More information on these datasets can be found at https://www.ncdc.noaa.gov/monitoring-references/faq/anomalies.php.

References

Androulidakis, Y.S., Kourafalou, V.H., 2011. Evolution of a buoyant outflow in the presence of complex topography: The Dardanelles plume (North Aegean Sea), *Journal of Geophysical Research: Oceans,* 116, C04019.

Androulidakis, Y.S., Krestenitis, Y.N., Kourafalou, V. H., 2012a. Connectivity of North Aegean circulation to the Black Sea water budget. *Continental Shelf Research*, *48*, 8-26.

Androulidakis, Y.S., Kourafalou, V.H., Krestenitis, Y.N., Zervakis, V., 2012b. Variability of deep water mass characteristics in the North Aegean Sea: The role of lateral inputs and atmospheric conditions. *Deep Sea Research Part I: Oceanographic Research Papers*, 67, 55-72.

de Boyer Montégut, C., Madec, G., Fischer, A.S., Lazar, A., Iudicone, D., 2004. Mixed layer depth over the global ocean: An examination of profile data and a profile-based climatology. *Journal of Geophysical Research: Oceans*, 109 (C12), C12003.

Cardin, V., Civitarese, G., Hainbucher, D., Bensi, M., Rubino, A., 2015. Thermohaline properties in the Eastern Mediterranean in the last three decades: is the basin returning to the pre-EMT situation? *Ocean Science,* 11 (1), 53-66.

Escudier, R., Clementi, E., Omar, M., Cipollone, A., Pistoia, J. *et al.,* 2020. Mediterranean Sea Physical Reanalysis (CMEMS MED-Currents) (Version 1) [Data set]. Copernicus Monitoring Environment Marine Service (CMEMS).

Kassis, D., Korres, G., 2020. Hydrography of the Eastern Mediterranean basin derived from argo floats profile data. *Deep Sea Research Part II Topical Studies Oceanography*, 171, 104712.

Kassis, D., Korres, G., Petihakis, G., Perivoliotis, L., 2015. Hydrodynamic variability of the Cretan Sea derived from Argo float profiles and multi-parametric buoy measurements during 2010-2012. *Ocean Dynamics*, 65 (12), 1585-1601.

Kassis, D., Krasakopoulou, E., Korres, G., Petihakis, G., Triantafyllou, G.S., 2016. Hydrodynamic features of the South Aegean Sea as derived from Argo T/S and dissolved oxygen profiles in the area. *Ocean Dynamics*, 1-18.

Kassis, D., Korres, G., Konstantinidou, A., Perivoliotis, L., 2017. Comparison of high resolution hydrodynamic model outputs with in-situ Argo profiles in the Ionian Sea. *Mediterranean Marine Science*, 18 (1), 22-37.

Klein, B., Roether, W., Manca, B.B., Bregant, D., Beitzel, V. *et al.,* 1999. The large deep water transient in the Eastern Mediterranean. *Deep Sea Research Part I: Oceanographic Research Papers*, 46 (3), 371-414.

Kourafalou, V.H., Barbopoulos, K., 2003. High resolution simulations on the North Aegean Sea seasonal circulation. *Annales Geophysicae,* 21 (1), 251-265.

Kress, N., Gertman, I., Herut, B., 2014. Temporal evolution of physical and chemical characteristics of the water column in the Easternmost Levantine basin (Eastern Mediterranean Sea) from 2002 to 2010. *Journal of Marine Systems*, 135, 6-13.

Lascaratos, A., Williams, R.G., Tragou, E., 1993. A mixed-layer study of the formation of Levantine intermediate water. *Journal of Geophysical Research Oceans* 98, 14739-14749.

Lascaratos, A., Roether, W., Nittis, K., Klein, B., 1999. Recent changes in deep water formation and spreading in the eastern Mediterranean Sea: a review. *Progress in Oceanography*, 44 (1-3), 5-36.

Malanotte-Rizzoli, P., Manca, B.B., d'Alcala, M.R., Theocharis, A., Brenner, S. *et al.,* 1999. The Eastern Mediterranean in the 80s and in the 90s: the big transition in the intermediate and deep circulations. *Dynamics of Atmospheres and Oceans*, 29 (2-4), 365-395.

Marshall, J., Schott, F., 1999. Open-ocean convection: Observations, theory, and models. *Reviews of Geophysics*, 37 (1), 1-64.

Nardelli, B.B., Tronconi, C., Pisano, A., Santoleri, R., 2013. High and Ultra-High resolution processing of satellite Sea Surface Temperature data over Southern European Seas in the framework of MyOcean project. Remote Sensing of Environment, 129, 1-16.

Ozer, T., Gertman, I., Kress, N., Silverman, J., Herut, B., 2017. Interannual thermohaline (1979-2014) and nutrient (2002–2014) dynamics in the Levantine surface and intermediate water masses, SE Mediterranean Sea. *Global and Planetary Change*, 151, 60-67.

Pisano, A., Nardelli, B.B., Tronconi, C., Santoleri, R., 2016. The new Mediterranean optimally interpolated pathfinder AVHRR SST Dataset (1982-2012). Remote Sensing of Environment, 176, 107-116.

Poulain, P., Barbanti, R., Font, J., Cruzado, A., Millot, C. *et al.,* 2007. MedArgo: a drifting profiler program in the Mediterranean Sea. *Ocean Science*, 3 (3), 379-395.

Riser, S.C., Freeland, H.J., Roemmich, D., Wijffels, S., Troisi, A. *et al.*, 2016. Fifteen years of ocean observations with the global Argo array. Nature Climate Change, 6, 145-153.

Roether, W., Manca, B.B., Klein, B., Bregant, D., Georgopoulos, D. *et al.,* 1996. Recent Changes in Eastern Mediterranean Deep Waters. *Science*, 271 (5247), 333-335.

Roether, W., Klein, B., Manca, B.B., Theocharis, A., Kioroglou, S., 2007. Transient Eastern Mediterranean deep waters in response to the massive dense-water output of the Aegean Sea in the1990s. Progress in Oceanography, 74 (4), 540-571.

Schroeder, K., Millot, C., Bengara, L., Ben Ismail, S., Bensi, M. *et al.,* 2013. Long-term monitoring programme of the hydrological variability in the Mediterranean Sea: a first overview of the HYDROCHANGES network. *Ocean Science,* 9 (2), 301-324.

Schroeder, K., Chiggiato, J., Josey, S.A., Borghini, M., Aracri, S. *et al.,* 2017. Rapid response to climate change in a marginal sea. *Scientific Reports*, 7 (1), 4065.

Skliris, N., 2014. Past, Present and Future Patterns of the Thermohaline Circulation and Characteristic Water Masses of the Mediterranean Sea. In *The Mediterranean Sea*. Springer, Dordrecht, pp. 29-48. Available at: https://link.springer.com/chapter/10.1007/978-94-007-6704-1_3 [Accessed July 23, 2018].

Theocharis, A., Georgopoulos, D., Lascaratos, A., Nittis, K., 1993. Water masses and circulation in the central region of the Eastern Mediterranean: Eastern Ionian, South Aegean and Northwest Levantine, 1986-1987. *Deep Sea Research Part II: Topical Studies in Oceanography*, 40 (6), 1121-1142.

Theocharis, A., Nittis, K., Kontoyiannis, H., Papageorgiou, E., Balopoulos, E., 1999. Climatic changes in the Aegean Sea influence the eastern Mediterranean thermohaline circulation (1986-1997). *Geophysical Research Letters*, 26 (11),

1617-1620.

Tragou, E., Zervakis, V., Papadopoulos, A., Maderich, V.S., Georgopoulos, D. *et al.,* 2003. Buoyancy transport through the Aegean Sea. In *2nd International Conference on "Oceanography of the Eastern Mediterranean and Black Sea: Similarities and Differences of Two Interconnected Basins* (pp. 38-46).

Tsimplis, M.N., Josey, S.A., 2001. Forcing of the Mediterranean Sea by atmospheric oscillations over the North Atlantic. *Geophysical Research Letters*, 28 (5), 803-806.

Tzali, M., Sofianos, S., Mantziafou, A., Skliris, N., 2010. Modelling the impact of Black Sea water inflow on the North Aegean Sea hydrodynamics. *Ocean Dynamics,* 60, 585-596.

Velaoras, D., Krokos, G., Nittis, K., Theocharis, A., 2014. Dense intermediate water outflow from the Cretan Sea: A salinity driven, recurrent phenomenon, connected to thermohaline circulation changes. *Journal of Geophysical Research: Oceans*, 119 (8), 4797-4820.

Velaoras, D., Krokos, G., Theocharis, A., 2015. Recurrent intrusions of transitional waters of Eastern Mediterranean origin in the Cretan Sea as a tracer of Aegean Sea dense water formation events. *Progress in Oceanography*, 135, 113-124.

Velaoras, D., Papadopoulos, V.P., Kontoyiannis, H., Papageorgiou, D.K., Pavlidou, A., 2017. The Response of the Aegean Sea (Eastern Mediterranean) to the Extreme 2016-2017 Winter. *Geophysical Research Letters*, 44 (18), 9416-9423.

Wong, A., Robert, K., Thierry, C., Argo Data Management Team, 2020. Argo Quality Control Manual for CTD and Trajectory Data.

Zervakis, V., Georgopoulos, D., Drakopoulos, P.G., 2000. The role of the North Aegean in triggering the recent Eastern Mediterranean climatic changes. *Journal of Geophysical Research: Oceans*, 105 (C11), 26103-26116.

Zervakis, V., Georgopoulos, D., 2002. Hydrology and circulation in the North Aegean (eastern Mediterranean) throughout 1997 and 1998. *Mediterranean Marine Science*, 3 (1), 7-21.

Zervakis V., Krasakopoulou E., Georgopoulos D., Souvermezoglou E., 2003. Vertical diffusion and oxygen consumption during stagnation periods in the deep north Aegean. *Deep Sea Research*, I 50, 53-71.